

Directional Modulation for Enhanced Privacy in Smartwatch Devices

Proposing a security solution compatible with Internet of Things devices.

Abel Zandamela¹, Nicola Marchetti², and Adam Narbudowicz³

This article studies the security aspects of data transmission in on-body Internet of Things (IoT) devices through the use of Directional Modulation (DM) from a smartwatch integrated antenna. DM is a beam steering-based Physical Layer Security (PLS) method used to transmit baseband constellations to known secure locations while simultaneously scrambling them in other directions. However, in the state of the art, DM is implemented using large arrays, which are outsized for many on-body IoT devices. To overcome this challenge, this study proposes multimodal ultrathin compact antennas suitable for integration into smartwatches. These antennas present advanced beam steering capabilities that allow the implementation of DM from a low-thickness structure of up to 0.57 mm or 1/100th of the wavelength at the center operating frequency. Two different DM implementations (simultaneous multipoint transmission and an energy-efficient single-port transmission) are tested using a multilayer phantom. Overall, secure steerable transmissions are realized, and experimental verifications are carried out to validate the proposed concept. Ultimately, this article demonstrates

Digital Object Identifier 10.1109/MAP.2024.3362150
Date of current version: 3 April 2024

EDITOR'S NOTE

This article for the "Bioelectromagnetics" column tackles security aspects for wearable Internet of Things (IoT) devices. The authors explore a smartwatch paradigm and demonstrate the use of a Directional Modulation (DM) approach implemented via miniaturized antennas. The approach is validated experimentally, ultimately opening new opportunities for low-cost and energy-efficient security techniques in wearables.

The "Bioelectromagnetics" column welcomes articles on biomedical applications of electromagnetics, antennas, and propagation in terms of research, education, outreach, and more. If you are interested in contributing, please e-mail me at kiourti.1@osu.edu.



Asimina Kiourti

the feasibility of applying new energy-efficient and low-cost security techniques to enhance the privacy of resource-constrained IoT devices.

INTRODUCTION

While still being a relatively nascent field, PLS allows one to complement the privacy of many cutting-edge wireless systems, like Multiple-Input, Multiple-Output (MIMO); the IoT; and others [1], [2], [3]. PLS techniques can provide additional protection against eavesdroppers by exploiting the physical characteristics of the wireless propagation channel, e.g., noise, fading, and interference. A potential area that can benefit from those methods is the growing field of wearable devices, where classical cryptography may

be unsuitable to implement due to tight energy and low processing power constraints [4].

Wearables are becoming indispensable to many modern applications, i.e., health-care and IoT systems [4], [5], [6]; however, they are susceptible to eavesdropping as the data transmission is done in an open wireless medium. The security issues are especially challenging for wearables as they also need to be compact to fit into body parts, e.g., human wrists and feet; therefore, small and low-profile antennas are desirable for integration into wearables. In addition, antennas for wearables need to account for coupling effects and efficiency deterioration due to the lossy human body [7], [8], [9]. Moreover, beam steering is desirable as this can allow

providing additional security through PLS methods like DM. The DM technique can enhance the privacy of wireless systems by optimizing the beam steering of arrays to transfer baseband constellation symbols to a prespecified secure direction while simultaneously distorting the same constellations in all other directions [10], [11].

To address wearable devices' security issues, this work introduces for the first time the use of DM from an ultrathin smartwatch antenna. The work also proposes a general framework for how DM can be used in compact IoT devices. Then, a discussion of the proposed multimodal antenna is presented, and beam steering characteristics are demonstrated across the entire azimuth plane using a model of only 0.024λ (1.34 mm) thickness, with further tuning demonstrated for 0.57 mm or 0.01λ (where λ is the wavelength at the center operating frequency, i.e., 5.57 GHz). Next, we evaluate the electromagnetic field exposure of the antenna by computing the Specific Absorption Rate (SAR) following the U.S. Federal Communications Commission (FCC) recommended setups for both the wrist-worn case and next-to-the-mouth conditions. Lastly, two DM implementations are tested in free space and with a multilayer phantom. The first DM scheme requires simultaneous multiport activation with

artificial noise, while the second DM approach needs only a single port activation without excessive artificial noise. The performance of both methods is investigated using full-wave simulations and validated through anechoic chamber measurements.

DM

In traditional beam steering, data transmission is done with the maximum power in the direction of the Legitimate User (LU), with the power in eavesdroppers' locations being as low as possible. The baseband constellations, i.e., the complex values in the In-phase Quadrature (IQ) plane, are the same for all transmitting directions of the antenna, as shown in Figure 1(a). This means that the differences between the directions are power levels and phase differences created by different propagation paths—both can be corrected by a reasonably advanced eavesdropper [2]. To enhance secrecy, the DM technique preserves the original Quadrature Amplitude Modulation (QAM) constellation in the desired LU direction, while at the same time, it spatially scrambles them in all other directions [see Figure 1(b)].

Babakhani et al. introduced in [12] the near-field direct antenna modulation using a driven dipole combined with passive reflectors. In [10], Daly and Bernhard demonstrated a similar secure modulation approach using a

four-element reconfigurable array. Hong et al. presented in [13] a dual-beam DM method; unlike [10] and [12], where the same antennas transmit the IQ patterns, in this approach, different antennas transmit the IQ patterns. Further research on DM is presented in [11], where Ding and Fusco introduced an orthogonal vector approach for DM transmitter (Tx) synthesis; in [14], Ding and Fusco also introduced a new type of DM Tx based on retro-directive arrays, where the injected orthogonal interference is not dependent on the preselected secure direction. Other contributions in the field are presented, e.g., in [15], [16], [17], [18], [19], [20], [21], [22], [23], [24], [25], [26], [27], [28], [29], [30], and [31]; phased arrays are used in [15]; switched antenna arrays are discussed in [16], [17], and [18]; multiuser MIMO DM systems are studied in [19], [21], and [23]; time-modulated arrays are investigated in [20] and [26]; hybrid MIMO phased arrays are studied for millimeter-wave communication systems in [25]; and dynamic multibeam DM using random changes of the artificial noise vector at the symbol rate is proposed in [22].

CHALLENGES AND LIMITATIONS OF DM FOR SMALL IoT DEVICES

Most DM schemes discussed previously are implemented using classical arrays. Since those typically require $\lambda/2$ interelement spacing, they

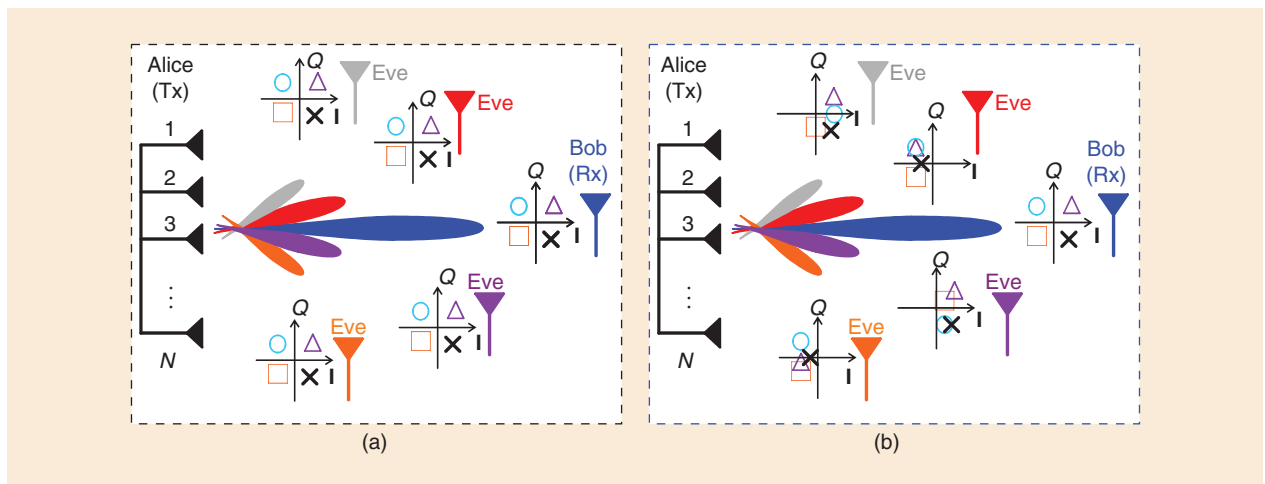


FIGURE 1. The visualization of (a) the traditional beam steering and (b) the DM method. The transmitter (Tx) Alice is an array comprising N -elements, Bob is the direction of the LU, and eavesdroppers (Eves) are located in different directions. Note that in the traditional beam steering, the IQ constellations are the same in all directions, while they are decipherable only in the Bob direction for the DM approach.

are challenging to use in wearable IoT systems. To address these issues, in this section, we first discuss MIMO antennas proposed for pattern diversity in smartwatches. Then, a review of DM implementations using compact antennas and recent advances in energy-efficient DM techniques are presented.

MIMO ANTENNAS FOR SMARTWATCH DEVICES

In recent years, different compact antennas have been proposed for smartwatch devices, e.g., in [32], [33], [34], [35], [36], [37], [38], [39], [40], [41], [42], [43], [44], [45], and [46]. Among those, MIMO designs have been studied in [41], [42], [43], [44], [45], and [46]. Wen et al. [44] exploited the theory of characteristics mode analysis to design a 7-mm-thick two-port MIMO antenna, with bidirectional and omnidirectional patterns, where the gain and efficiency drop from 3.5 dBi and 75% (free space) to 2 dBi and 42% (with hand phantom). In [46], Liao et al. investigate an 8-mm-thick L-shaped slot and loop-based MIMO antenna, covering five different bands, with an efficiency >25% when tested on a hand phantom. Other MIMO smartwatch designs are discussed, e.g., in [41] (two-port MIMO design based on a folded monopole with a thickness of 5 mm); in [42] (a 5.4-mm-thick two-port MIMO based on the inverted-F antenna); in [43] (a 5-mm-thick three-port multiband MIMO design); and in [45] (7.5-mm-thick two-port MIMO based on an annular ring).

While the aforementioned works show significant improvements in their pattern diversity and other antenna performance, they still have a large profile. More importantly, their beamforming performance is limited for DM implementation (as the desired secure direction of the LU can be in any direction in the 3D space). This means that the beamforming of the antenna should allow the main beam to be pointed at the LU and maintain the true constellation in that direction [see Figure 1(b)], while the signal in other directions is weak and the constellation symbols are distorted. However, such performance cannot be realized

using the beamforming of the works discussed previously.

DM FROM COMPACT ANTENNAS AND ENERGY-EFFICIENT DM SCHEMES

In recent years, only a few works have proposed DM schemes in small IoT devices. Narbudowicz et al. [27] introduced a compact DM system using a dual-mode antenna of $\lambda/2$ diameter and 0.31λ profile. Parron et al. [28] proposed a four-mode stacked patch design of diameter 0.7λ and 0.05λ profile. Although a low-profile design is achieved in [28], high side lobes are present, which can compromise the security of the transmitted data. Moreover, the solution uses a stacked patch approach, and similarly to [27], such designs are challenging for smartwatch devices' packaging. The work in [29] proposes a DM method using a $3\lambda/2$ switched dipole antenna; however, it is still too bulky for integration into smartwatch devices. Recently, in [30], we proposed a five-mode antenna (0.65λ diameter and 0.19λ profile) capable of unique steerable DM transmissions without high side lobes. However, the profile is still relatively high for wrist-wearable IoT devices. In addition, like [27] and [28], it is a stacked patch antenna, which presents challenges for smartwatch packaging as typically very low-profile antennas are desirable to allow for the placement of other smartwatch components, such as the battery, LCD, heart rate monitor, and others.

A few approaches have been proposed to improve the energy efficiency of DM techniques, e.g., RF power amplifier efficiency [47]; power efficiency and security of QAM and amplitude and phase-shift keying DM systems [48]; time-modulated phased arrays requiring only a single active RF chain [49]; and reconfigurable power dividers [50]. While the aforementioned methods present significant breakthroughs, their implementation for small IoT devices is not feasible due to the higher computational demands and the requirement of sophisticated switching sequences with careful synchronization. In our recent work [31], we propose a simple single active RF-chain DM scheme, where the switch-

ing sequence can be fully random and independent of the direction of the LU. Nevertheless, the implementation uses a five-element array, which is still a large diameter and profile for smartwatch device packaging.

ULTRATHIN MULTIMODAL ANTENNAS FOR DM IN SMARTWATCHES

The proposed multimodal antenna is shown in Figure 2 and operates near 5.57 GHz and is 1.34 mm thick with a 33-mm diameter ($0.61\lambda \times 0.61\lambda \times 0.024\lambda$). The design uses a single layer of Rogers TMM6 substrate ($\epsilon_r = 6$, $\tan \delta = 0.0023$) and comprises two concentric shorted ring structures fed using three ports to excite different orthogonal modes. The inner ring is fed using P1 and includes eight shorting pins rotated by 45° with respect to the center. Due to the inductance of the pins, an increase in the resonance frequency is observed compared to the case without the pins. The outer ring is fed using P2 and P3, and it includes 16 pins rotated by 22.5° with respect to the center. In both rings, the pins are placed at a distance v_1 from the inner radius. Note that good isolation and frequency tuning can be obtained by controlling the total number of pins and the value v_1 ; in general, the higher the number of pins and v_1 , the larger frequency shift is obtained. The parameter v_1 is optimized to 1 mm for both rings, and the number of pins is selected, taking into account the symmetry between the feeding ports. The antenna is simulated in free space using a finite element method-based 3D full-wave solver. The electric field distribution for each port is shown in Figure 3. It is seen that P1 excites a monopolar-like pattern, while P2 and P3 excite two orthogonal modes of the same order; the mode purity of each excited pattern compared to the respective ideal spherical mode pattern is above 98% for all the ports.

Next, a hand phantom based on the computed tomography results of [51] is used to evaluate the performance on the user's wrist. The phantom comprises four layers (see Figure 4), with the skin and the fat layers occupying 15% of the total volume; the muscle layer occupying 72.1%; and the bone layer occupying 12.9%. The respective

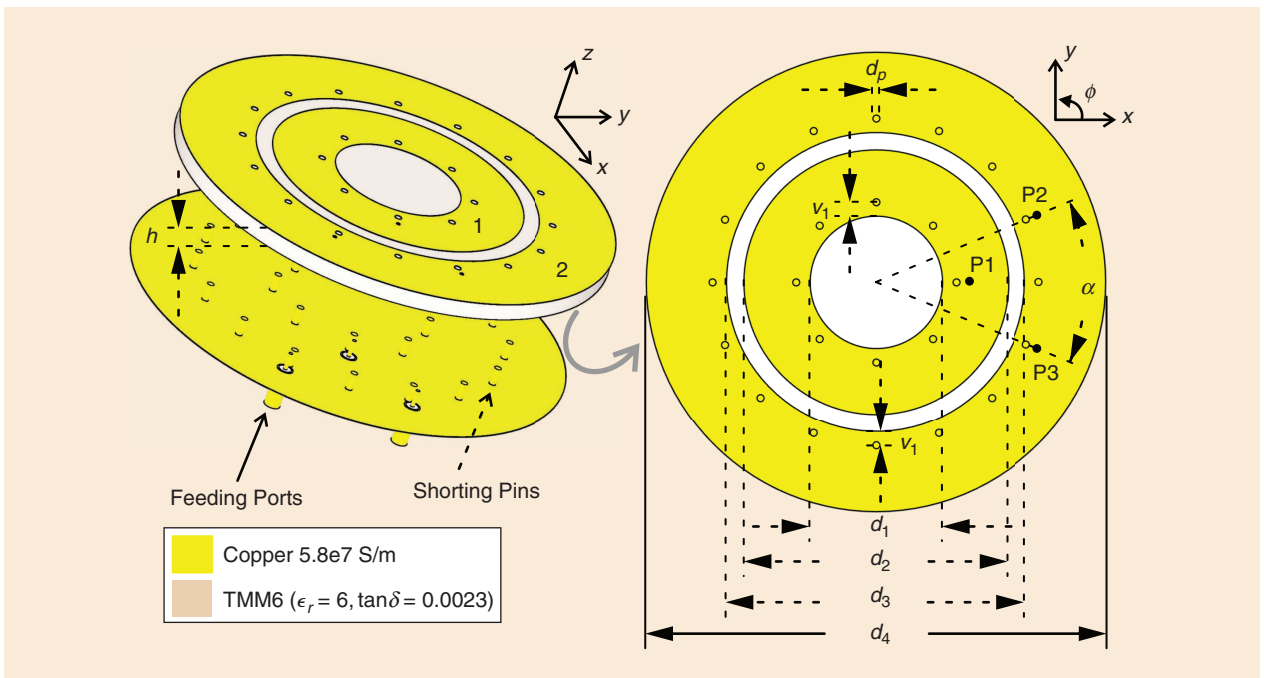


FIGURE 2. The proposed antenna, design A; dimensions (all in mm): $h = 1.27$, $d_1 = 10$, $d_2 = 18$, $d_3 = 21.5$, $d_4 = 33$, $d_p = 0.5$, $v_1 = 1$, $\alpha = 45^\circ$ (135°). Feed points: P1 = 7, P2 = P3 = 12.5.

dielectric properties of each layer are obtained from [52]. To evaluate the antenna performance in a realistic scenario, a pig's foot of length 205 mm is used as the phantom. The manufactured prototype is shown in Figure 4; and in both cases (simulated and measured), the antenna is placed in direct contact (i.e., 0-mm separation) with the skin layer of either the phantom or the pigs' foot. Note that this setup

assumes the worst-case scenario (antenna in direct contact with the lossy hand phantom or pigs' foot); the implication is that a much larger efficiency drop will occur in our proposed setup due to the antenna's close proximity to the phantom. However, its ultrathin properties allow placement at different heights inside the smartwatch housing.

The antenna offers good isolation characteristics owing to the orthogonal-

ity of the excited modes. The isolation is better than 29 dB [free space; Figure 5(a)] and 15 dB [including phantom; Figure 5(c)] for the simulated case. For the measured case, the isolation is better than 15 dB [free space; Figure 5(b)] and 12 dB [including phantom; Figure 5(d)]. Note that a frequency shift is observed between the simulated and measured cases in free space, from 5.57 GHz (simulations) to 5.73 GHz (measurements); this is most likely due to the combined effect of the substrate permittivity and fabrication tolerances. In addition, the setup with the hand phantom shows a small shift toward lower frequencies from 5.73 GHz [Figure 5(b)] to 5.71 GHz [Figure 5(d)]. At the center frequency of each case, the antenna total efficiency in free space is 76% (for P1) and 57% (for P2 and P3)—changing to 52% (for P1) and 41% (for P2 and P3) when including the phantom. The measured -10 -dB Impedance Bandwidth (IBW) is 41.4 MHz (free space) and 37.6 MHz (including the phantom).

Lastly, to test the effect of different smartwatch components, lossy metals with a dielectric shell ($\epsilon_r = 1.5$) are used to simulate a 0.7-mm-thick Printed Circuit Board Assembly (PCBA) and a 3-mm-thick battery [see Figure 6(a)].

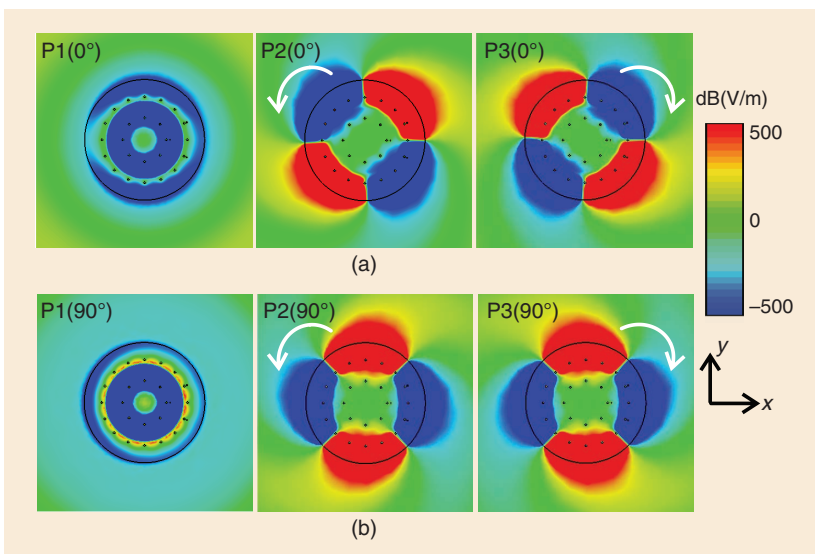


FIGURE 3. E-field distribution (z -components) for each port of the proposed multimodal ultrathin antenna. (a) 0° phase. (b) 90° phase.

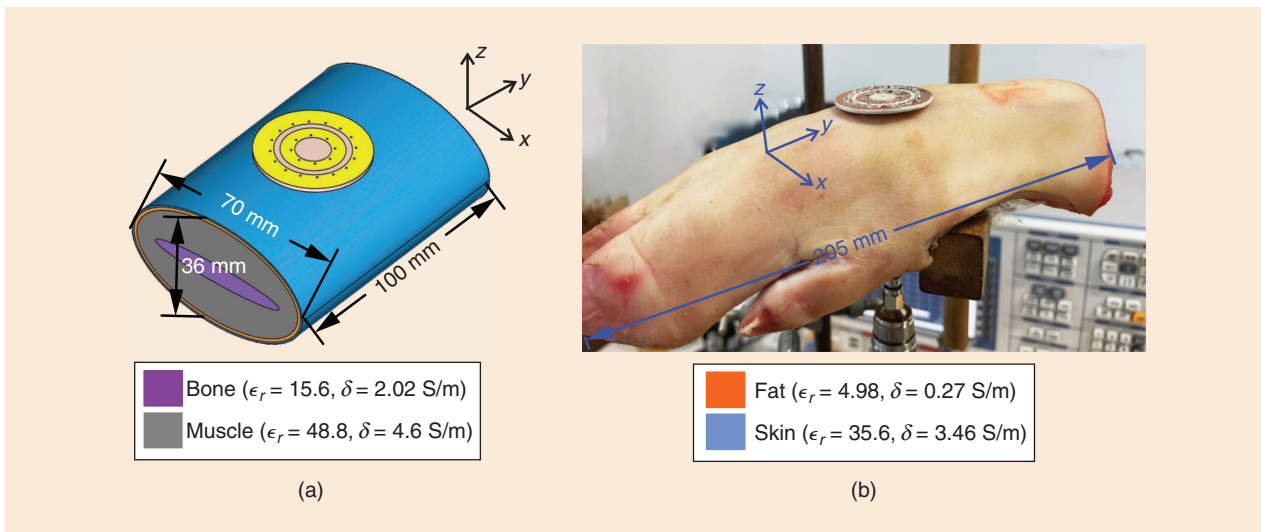


FIGURE 4. Proposed setups. (a) Users' wrist scenario where the antenna is placed in direct contact with the skin layer of the phantom. (b) A measurement setup using a pig's foot of length 205 mm, with a width and thickness of approximately 50 mm.

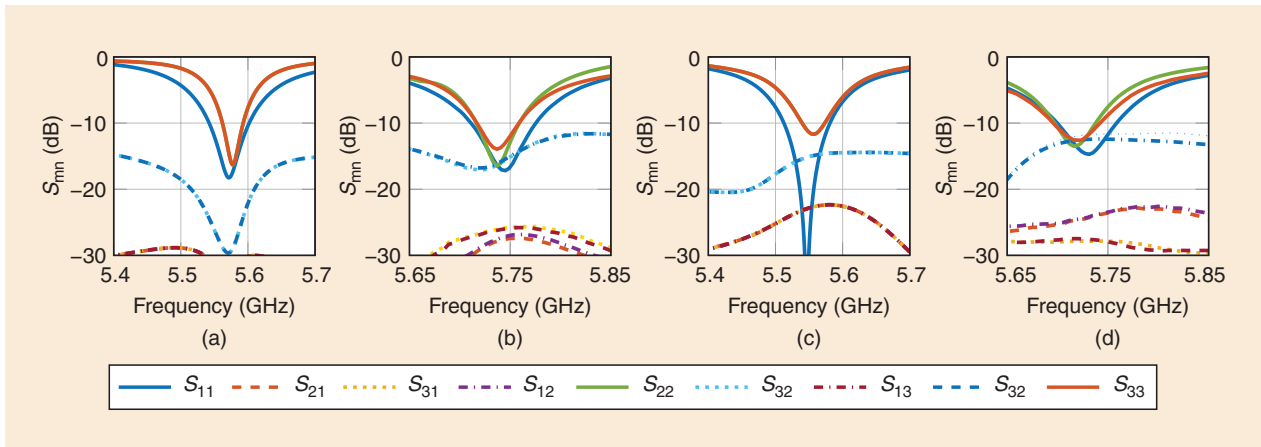


FIGURE 5. The S-parameters results. (a) Simulated free space. (b) Measured free space. (c) Simulated with hand phantom. (d) Measured with hand phantom.

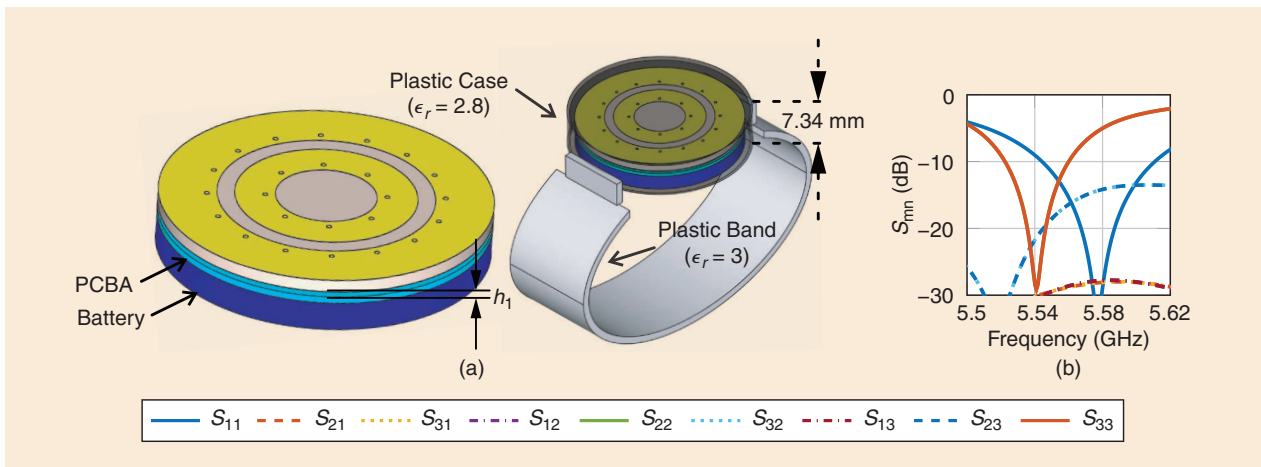


FIGURE 6. An antenna with smartwatch components. (a) An antenna tested with a PCBA, battery, plastic housing of a 7.34-mm thickness, and plastic wristband, where $h_1 = 0.5$ mm. (b) The S-parameters results.

The antenna, PCBA, and battery are placed inside a plastic case, where a 1-mm gap between all the components and the housing is introduced. A plastic band of width 20 mm, with 14-mm rectangular end strips, is connected at two opposite sides of the plastic housing [see Figure 6(a)]. The S-parameter results are shown in Figure 6(b). For this case, P2 and P3 have a small downward frequency shift, which, however, can be easily tuned, depending on the final design of the commercial product. Nevertheless, the \vec{E} -field patterns have similar characteristics with the free space results, and an overlap -10-dB bandwidth of 14 MHz is realized.

ANTENNA PATTERN PERFORMANCE ON GUSTAV VOXEL MODEL AND SAR ANALYSIS

To test the antenna pattern on a realistic human model, the multimodal design was simulated with the CST Studio Suite Gustav voxel model. The patterns were tested in two different setups: a hand along the body [Figure 7(a)] and the elevated hand case [Figure 7(b)]. It can be seen that small pattern deformities and deepes are present, especially for directions that lie along the hands' length. Such deformities are mostly due to the voxel model electromagnetic absorption and reflections from its surface. Note that those small deepes occur mostly around the +y direc-

tion, i.e., toward the voxel model. Because it is often desired to radiate away from the body, the beam steering toward the -y direction is still realized. In general, all three ports still present the required pattern properties to allow for good beam-forming characteristics.

Because the antenna is proposed to operate on a human wrist, we analyzed the electromagnetic field exposure by computing the SAR. The calculations were done following the FCC guidelines under two conditions: the first is the wrist-worn case, where the device is placed in direct contact with a block filled with human hand tissue ($\epsilon_r = 21.1$, $\delta = 0.52$, and $\rho = 1,000 \text{ kg/m}^3$) and averaged in 10 g; the second case is the next-to-the-mouth one, with the device placed at a 10-mm distance from a block filled with human head tissue ($\epsilon_r = 35.1$, $\delta = 5.3$, and $\rho = 1,000 \text{ kg/m}^3$) and 1 g of averaging. An input power of 10 mW is used, and for the wrist-worn condition, the largest value of the SAR between all the ports is 0.073 W/kg [see Figure 8(a)], which is still well below the FCC limits of 4 W/kg. For the next-to-the-mouth condition, the largest SAR is 0.22 W/kg [see Figure 8(b)], also staying well below the 1.6 W/kg limit.

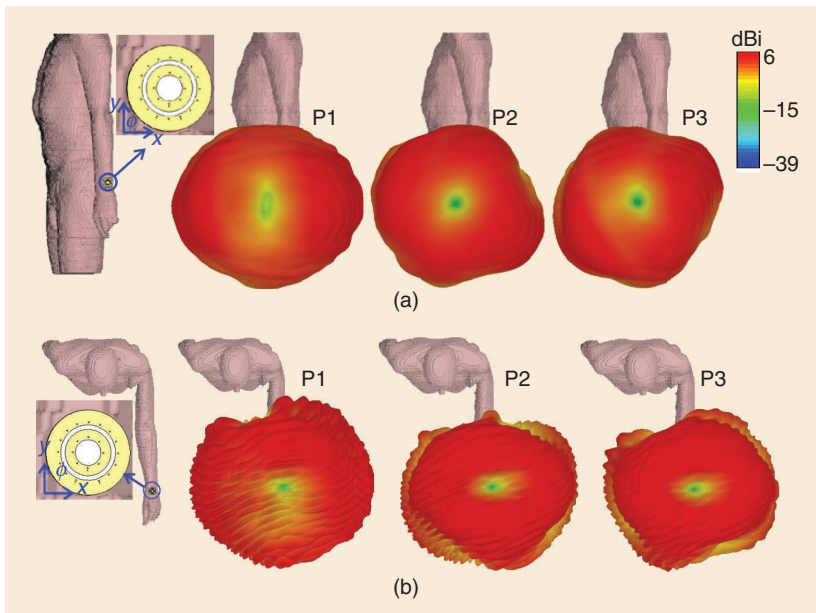


FIGURE 7. The antenna directivity patterns on the Gustav voxel model. (a) The setup with the hand along the body. (b) The setup with the elevated hand.

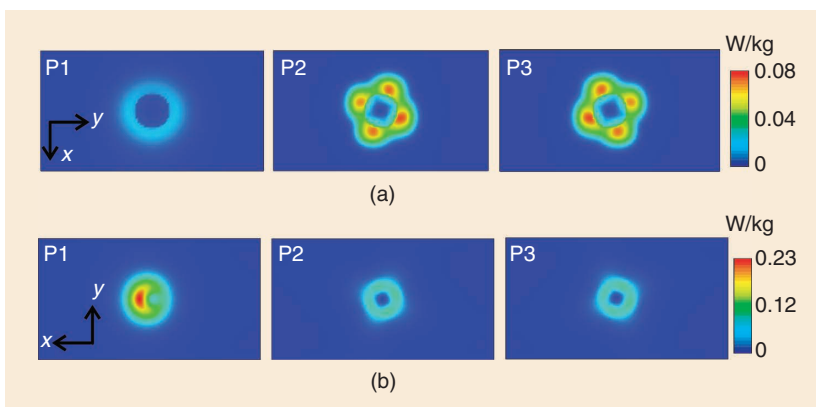


FIGURE 8. The antenna SAR results following the FCC guidelines. (a) The wrist-worn setup. (b) The next-to-the-mouth setup.

CALCULATED BEAM STEERING RESULTS

To realize beam steering within size-constrained spaces, the proposed multimodal ultrathin antenna exploits the different phase variations of each radiated mode—the method is detailed in [53]—and it is based on the fact that the \vec{E} -field at a large distance ($kr \rightarrow \infty$) can be expressed as a weighted sum of the far-field spherical wave pattern functions \vec{K}_{smn} defined as [54]

$$\vec{E}(r, \theta, \phi) = \sqrt{\eta} \frac{k}{\sqrt{4\pi}} \frac{e^{ikr}}{kr} \times \sum_{smn} Q_{smn} \vec{K}_{smn}(\theta, \phi) \quad (1)$$

where η is the specific impedance of the medium, $k = 2\pi/\lambda$ is the specific wavenumber, and Q_{smn} are the spherical modes' coefficients. s represents the polarization, where for the TM modes $s = 1$ is proportional to the \vec{H} -fields, and $s = 2$ is proportional to the \vec{E} -fields, and

the opposite is true for the TE modes. The indices (m, n) , with $|m| \leq n$, indicate the azimuthal phase change and the order of the spherical mode, respectively. The spherical wave functions $\tilde{K}_{smn}(\theta, \phi)$ are power-normalized dimensionless solutions of the vector wave equation. For the proposed beam steering principle, the modes of interest are of type $s = 1$, and assuming $e^{-i\omega t}$ time dependency, they are given as

$$\tilde{K}_{1mn}(\theta, \phi) = \frac{1}{\sqrt{2\pi}} \frac{1}{\sqrt{n(n+1)}} \left(-\frac{m}{|m|}\right)^m \times e^{im\phi} \left\{ \frac{im\tilde{P}_n^{|m|}(\cos\theta)}{\sin\theta} \tilde{e}_\theta - \frac{d\tilde{P}_n^{|m|}(\cos\theta)}{d\theta} \tilde{e}_\phi \right\} \quad (2)$$

where $\tilde{P}_n^{|m|}\cos\theta$ is the normalized associated Legendre function. To realize the proposed beam steering, the \tilde{K}_{1mn} modes can have a different order, i.e., $n = 1, 2, 3, \dots, N$. Next, the order of the modes excited by the largest ring is assumed to be the highest order that can be excited in the structure, and then, all the lowest order modes

are also excited using the remaining rings. All the modes are required to be omnidirectional (see Figure 9) with different azimuthal phase variations m . From (2), the modes generated by each port of the proposed antenna are shown in Figure 10(b) and can be classified as P1 $\rightarrow \tilde{K}_{1,0,1}$, P2 $\rightarrow \tilde{K}_{1,-2,2}$, and P3 $\rightarrow \tilde{K}_{1,+2,2}$. The phase of the pattern radiated by ring 1 is monopole like, i.e., with constant phase across the entire azimuth plane ($m = 0$), while the phase changes twice for ring 2 ($m = \pm 2$). Note that the phases of ring 2 change in two opposing directions, i.e., the “+” sign indicates the clockwise direction, and the “-” sign is the counterclockwise direction. These properties are exploited to create constructive interference in the desired directions by means of phase control, allowing for beam steering while using a compact size with a thickness suitable for smart-watch device packaging.

To evaluate the proposed beam steering principle, measurements were performed in an anechoic chamber both in free space and with the phan-

tom. The measurement setup is shown in Figure 9(a). The free space patterns for each port are shown in Figure 9(b) (simulated case) and Figure 9(c) (measured case); it is seen that a good agreement is achieved with both cases, showing omnidirectional patterns for each antenna port. Figure 9(d) shows the simulated patterns with the phantom, and their counterpart measured results are shown in Figure 9(e); it is observed that some shouldering and deeps are present in the measured case. This discrepancy may be due to the reflections of the antenna holder and other pig’s foot assembly components during measurements. The beam steering performance in free space is shown in Figure 9(f), and the results, including the phantom, are shown in Figure 9(g). It is seen that for both cases, a bidirectional pattern is realized, and the desired main beam directions are in good agreement with the simulated cases. The input amplitude (A_{inp}) and phase shift (Δ_{ph}) for each port of the generated beams are shown in Table 1.

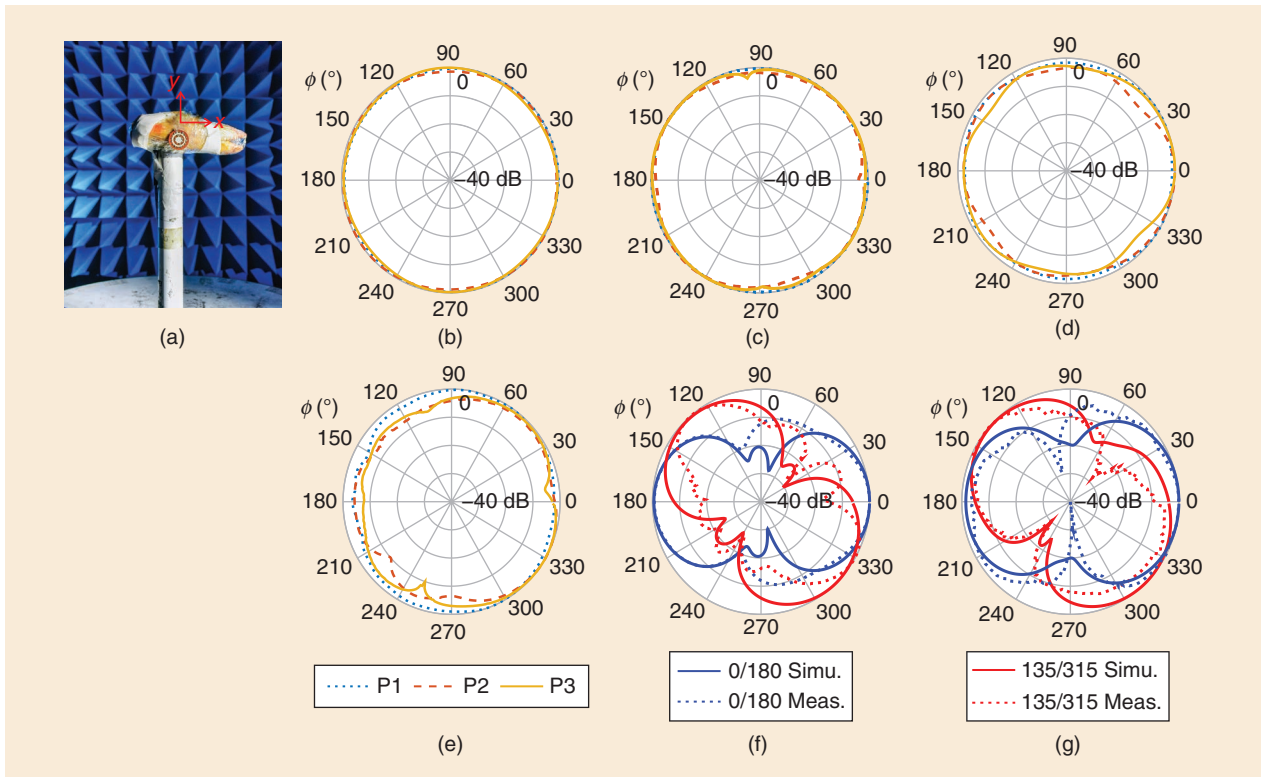


FIGURE 9. Normalized patterns. (a) The anechoic chamber measurement setup with the pig’s foot. (b) Free space simulated (Sim.) results. (c) Free space measured (Meas.) results. (d) Simulations with the phantom. (e) Measurements with the phantom. (f) Free space beam steering, (g) Beam steering results with the phantom.

TUNING CAPABILITIES OF THE ULTRATHIN MULTIMODAL DESIGN

The proposed beam steering principle allows for a wide tuning range of the antenna parameters. To highlight such design flexibility, Figure 10(a) (left)

shows a variation of the antenna shown in Figure 2. The new antenna (design B) uses the same diameter as design A (Figure 2) but is loaded with TMM10 substrate, with $\epsilon_r = 10$ (as compared to design A, with TMM6 and $\epsilon_r = 6$). This

allows further miniaturization as the center frequency shifts from 5.57 GHz (design A) to 4.48 GHz (design B). Note that due to miniaturization, the total efficiency drops to around 36.5% (57% in design A), and the isolation is better than 25 dB. The thickness of the substrate material of the antenna can also be tuned, as shown in Figure 10(a) (right), i.e., design C, which uses a substrate thickness of 0.5 mm, and the total antenna thickness is then 0.57 mm.

Figure 10(b) shows design D, which is capable of unidirectional beam steering around the azimuth plane. This is achieved by adding a new ring exciting $\tilde{K}_{1,-3,3}$ and $\tilde{K}_{1,+3,3}$ modes; therefore, a total of five modes are combined for beam steering, i.e., $m = 0$ (constant phase), $m = \pm 2$ (dual-azimuthal phase change), and $m = \pm 3$ (triple-azimuthal phase change). Note that the three-ring antenna uses the lowest number of modes that can allow for unidirectional beam steering around the desired plane. Lastly, a comparison of the four different designs is shown in Table 2. Note that because of the good tradeoff offered by design A (in terms of size, efficiency, and beam steering), all the DM results discussed in the following section are calculated using this model.

Beam Direction	P1 (A_{inp})	P1 (Δ_{ph})	P2 (A_{inp})	P2 (Δ_{ph})	P3 (A_{inp})	P3 (Δ_{ph})
0°/180° (free space)	1	0°	1	68°	1	-23°
135°/315° (free space)	1	0°	1	-23°	1	70°
0°/180° (phantom)	1	0°	1	33°	1	33°
135°/315° (phantom)	1	0°	1	-55°	1	-245°

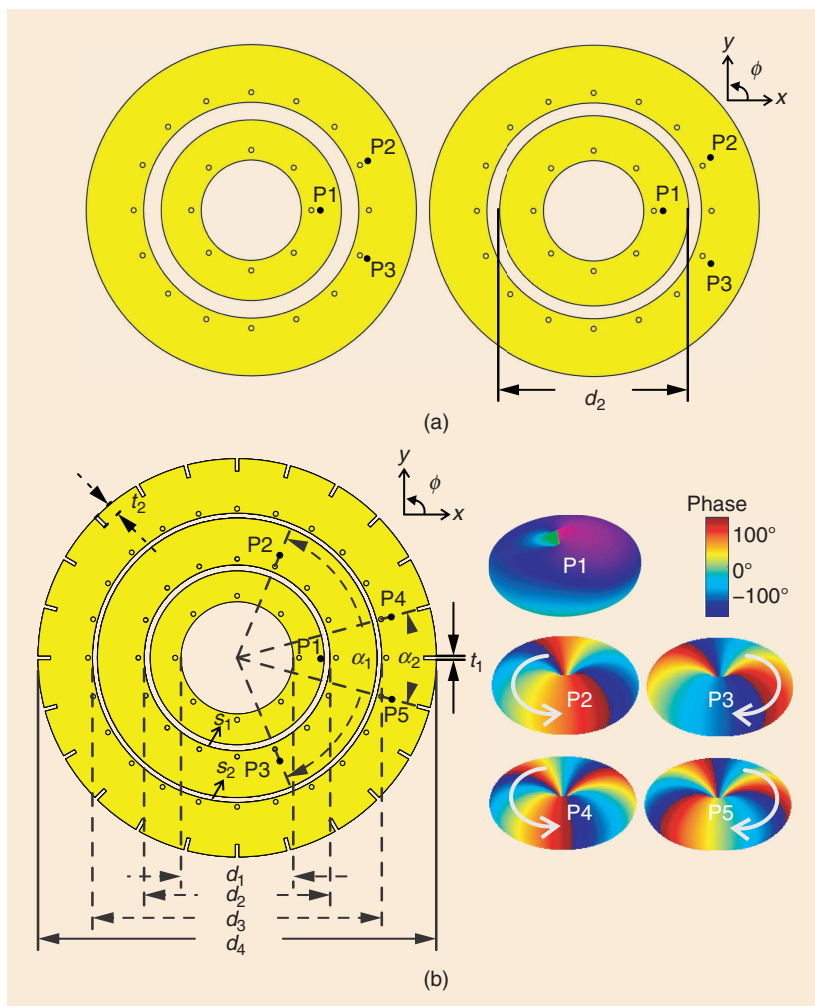


FIGURE 10. Multimodal antennas, all dimensions in mm. (a) The left image shows design B ($P1 = 7, P2 = , P3 = 12.75$), and the right image shows design C ($P1 = 7, P2 = , P3 = 12.75, d_2 = 18.95$). (b) The left image shows design D [$d_1 = 11.56, d_2 = 19.16, d_3 = 29.8, d_4 = 41, s_1 = 0.64, s_2 = 0.52, t_1 = 0.4, t_2 = 1.3, \alpha_1 = 135^\circ (45^\circ), \alpha_2 = 30^\circ (90^\circ), P1 = 8.6, P2 = 11.5, P3 = 11.5, P4 = 16.5, \text{ and } P5 = 16.5$, the remainder of the dimensions follow design A]; the right image shows the phase of the radiation patterns of the proposed designs.

DM FROM ULTRATHIN MULTIMODAL ANTENNAS

PROPOSED DM SCHEMES

Two DM schemes are studied with the proposed antenna. In scheme 1, all the complex patterns generated by exciting each port are used as DM weights, and artificial noise is added to scramble the IQ constellations in all undesired directions [53]. In scheme 2, only the complex patterns generated by a single port are used, with no excessive artificial noise in undesired directions [31].

Without loss of generality, we will use Quadrature Phase-Shift Keying (QPSK), and it is assumed that the transmitted signal propagates through a line-of-sight channel; the DM schemes are evaluated as follows:

- 1) First, the far-field results of design A (Figure 2) are obtained from a 3D full-wave solver or through anechoic

chamber measurements. The complex patterns of the antenna are extracted in free space, including the wrist phantom or pig's foot (see Figure 5).

- 2) The DM transmissions are studied for the entire azimuth plane; i.e., the elevation angle is fixed at $\theta = 90^\circ$, with the azimuth angles ϕ having a 1° resolution.
- 3) Next, the DM schemes are implemented using MATLAB; a symbol is modulated using QPSK, and the resulting complex data symbol is denoted as $d \in \{1; j; -1; -j\}$.
- 4) For scheme 1
 - A random complex vector \vec{s}' composed of $N/2$ elements (where N is the total number of ports in the antenna) is drawn with uniform distribution from $[-1, 1]$ and $[-j, j]$.
 - Next, to scatter the constellation symbols, a vector \vec{s} comprising N -elements is obtained from a random permutation of the elements of the vector \vec{s}' and its negation, giving $\sum_{n=0}^{N-1} \vec{s}_n = 0$, ensuring random noise cancellation in the desired secure direction. In addition, the permutation avoids any regularity that can be exploited by eavesdroppers as random values will be assigned to different antenna ports.
 - Next, the vector \vec{m} is formed by adding the modulated symbol d to each element of \vec{s} .
 - Then, the transmitted signal precoding is applied through zero-forcing. Each element is then communicated by the complex pattern excited by each respective antenna port.
 - Lastly, Additive White Gaussian Noise (AWGN) is added at the receiver (Rx) and is assumed to be independent at each location.
- 5) For scheme 2
 - First, a random number generator is used to select the reference port to establish the handshake; this step should be done as often as possible for increased security.
 - Then, phase compensation is added in the desired direction

of the LU to account for phase variation when switching between antenna ports, while random phase changes are observed in any other direction.

- AWGN is added at the Rx and is assumed to be independent in each direction.
- 6) Both DM schemes are tested using 10^5 transmitted symbols and a Signal-to-Noise Ratio (SNR) of 12 dB, and the performance is evaluated through Bit Error Rate (BER) calculations.

DM PERFORMANCE

Figure 11(a) shows the DM concept for the users' wrist scenario, where the IQ constellations are only decipherable in the Bob direction. Figure 11(b)–(e) shows the BER performance for schemes 1 and 2 at the center frequency of each case. In all four cases, the transmissions are tested for two different directions of the LU: $\phi_{\text{Bob}} = 45^\circ$ and $\phi_{\text{Bob}} = 135^\circ$. The DM performance in free space is shown in Figure 11(b) (for $\phi_{\text{Bob}} = 45^\circ$) and Figure 11(c) (for $\phi_{\text{Bob}} = 135^\circ$). It is seen that very low BER values are realized at the desired LU directions for both schemes; however, it should be noted that due to the bidirectional beam steering of design A, a second direction with low BER values is observed at $\phi_{\text{Bob}} + 180^\circ$. Nevertheless, design D [Figure 10(b)] can be used for applications requiring unique secure transmissions across the entire azimuth plane. The DM performance for the users' wrist scenario is shown in Figure 11(d) (for $\phi_{\text{Bob}} = 45^\circ$) and Figure 11(e) (for

$\phi_{\text{Bob}} = 135^\circ$); good agreement is also obtained with very low BER values at the desired LU directions.

For the free space case, the largest BER $< 10^{-2}$ beamwidth for the investigated LU directions is 60° for scheme 1 and 13° for scheme 2. These values change to 53° for scheme 1 and 14° for scheme 2 when evaluated in the users' wrist scenario. Overall, these results demonstrate that in all the investigated cases, the BER beamwidth for scheme 2 is much narrower (approximately four times narrower) compared to the beamwidth obtained with scheme 1. This translates into increased privacy as the decipherable IQ constellations are transmitted in a much smaller region, limiting the possibility of eavesdroppers to access the information. This performance also highlights that secure transmissions are realized without the simultaneous activation of multiple ports, which reduces the energy consumption in smartwatches as only a single port is active at a time. The proposed techniques are therefore expected to bridge the current gap between the security issues of on-body wearable IoT devices and low-computational power requirements, e.g., in off-body communications of many emerging applications like the Internet of Medical Things.

CONCLUSION

This article addressed the DM from resource-constrained wrist-worn IoT devices. Firstly, it provided an overview of the DM PLS technique. Then, it proposed a compact and IoT-compatible solution that allows

TABLE 2. ANALYSIS OF THE TUNING CAPABILITIES OF THE PROPOSED PRINCIPLE.

Design	f_0 (GHz)	Size	ϵ_r	S_{mn} (dB)	-10 dB IBW (MHz)	Tot. Eff. (%)
A	5.57	$0.61\lambda \times 0.61\lambda \times 0.024\lambda$	6	>29	31	57
B	4.48	$0.49\lambda \times 0.49\lambda \times 0.02\lambda$	10	>25	7	36.5
C	5.51	$0.6\lambda \times 0.6\lambda \times 0.01\lambda$	6	>25	25	26.6
D	5.77	$0.78\lambda \times 0.78\lambda \times 0.02\lambda$	6	>21.6	25	45.5

Tot. Eff.: total efficiency.

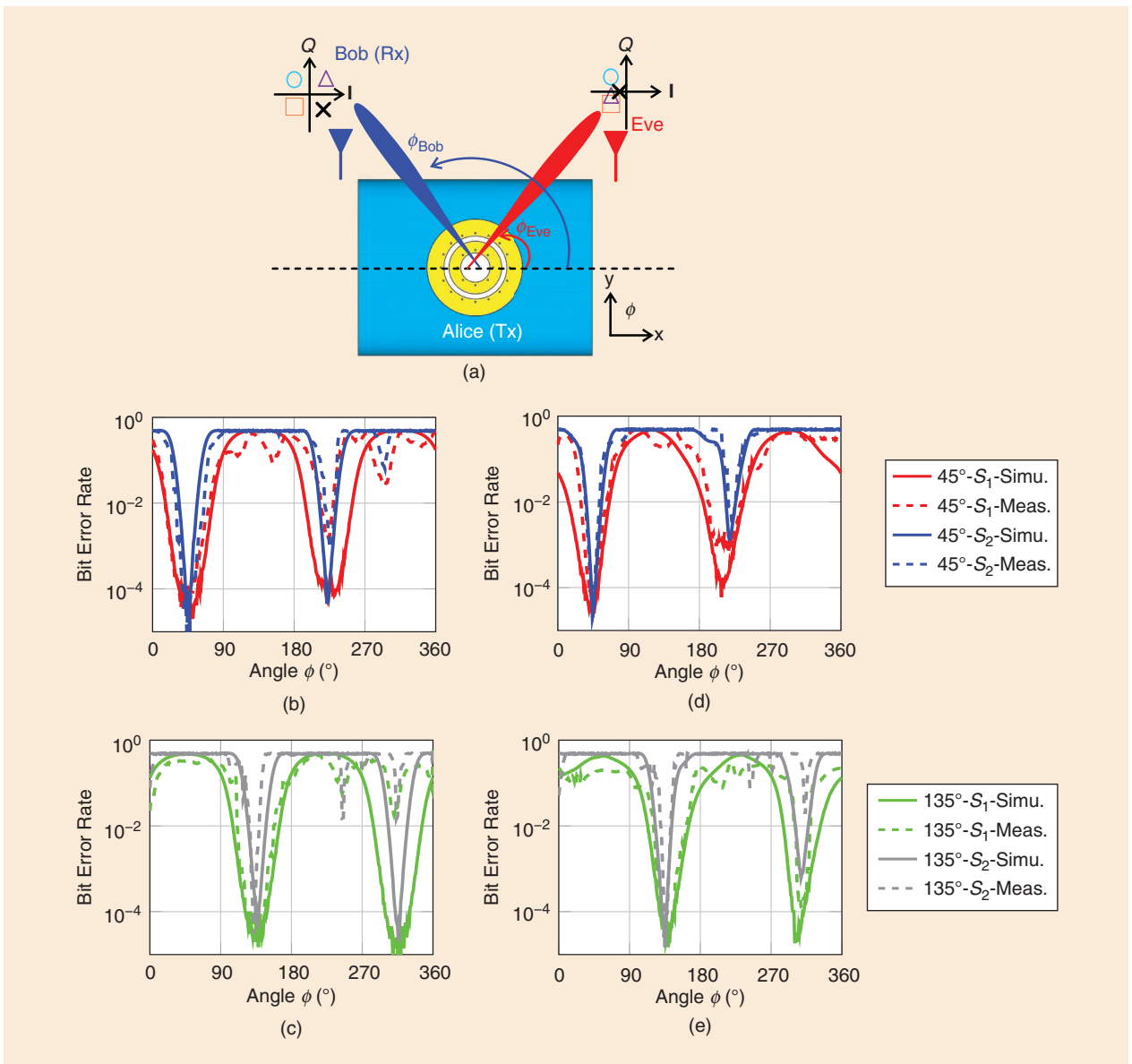


FIGURE 11. The BER calculations. (a) The proposed DM scheme for users' wrist scenario, where the multimodal antenna (Alice) is the transmitter, the desired secure transmission direction is the Bob direction (ϕ_{Bob}), while eavesdroppers (Eve) are present in the azimuth plane (xy -plane), and S1 represents scheme 1, while S2 is scheme 2. (b) Free space DM results for a 12-dB SNR scenario for $\phi_{Bob} = 45^\circ$: simulated case (solid lines) and measured case (dashed lines). (c) Free space results for $\phi_{Bob} = 135^\circ$. (d) DM results for the users' wrist scenario for $\phi_{Bob} = 45^\circ$. (e) The users' wrist scenario for $\phi_{Bob} = 135^\circ$.

us, for the first time, to effectively use such techniques from smart-watch devices. This functionality was made possible by recent advances in ultrathin antenna technology, integrated into constrained spaces and operating efficiently in proximity to the human body. By exploiting the phase characteristics of the antenna, one can realize beam steering properties to cover the entire azimuth plane with a low-profile structure of 1.34 mm, with further tuning capa-

bility to 0.57 mm. This beam steering capability is subsequently used to execute the DM security scheme. The technique further addressed current challenges posed by smartwatch energy constraints by enabling the implementation of an energy-efficient single-RF-chain DM scheme. The proposed work can significantly contribute to the new area of PLS for wearable IoT devices thanks to its capability for miniaturization and the use of single-RF-chain techniques.

ACKNOWLEDGMENT

This publication has emanated from research conducted with the financial support of Science Foundation Ireland under Grant number 18/SIRG/5612.

AUTHOR INFORMATION

Abel Zandamela (zandamea@tcd.ie) is currently pursuing his Ph.D. degree in electronic and electrical engineering at the CONNECT Centre, Trinity College Dublin, College Green, Dublin 2, Ireland. His research interests include

electrically small antennas, beam steering antennas, wireless physical layer security, on-body antennas, Internet of Things localization, and leaky-wave antennas. He is a Graduate Student Member of IEEE.

Nicola Marchetti (nicola.marchetti@tcd.ie) is an associate professor in wireless communications at the CONNECT Centre, Trinity College Dublin, College Green, Dublin 2, Ireland, where he leads the Wireless Engineering and Complexity Science lab (WhyCOM). He is an IEEE Communications Society Distinguished Lecturer and a Fellow of Trinity College Dublin. He is a Senior Member of IEEE.

Adam Narbudowicz (narbudoa@tcd.ie) is a senior researcher at the CONNECT Centre, Trinity College Dublin, College Green, Dublin 2, Ireland, and a part-time associate professor at the Wroclaw University of Science and Technology, 50-370 Wroclaw, Poland. His research interests include antenna miniaturization and reconfigurable antenna, sustainable antenna technology, and the use of machine learning for radar applications. He is a Senior Member of IEEE.

REFERENCES

- [1] X. Chen et al., "A survey on multiple-antenna techniques for physical layer security," *IEEE Commun. Surveys Tuts.*, vol. 19, no. 2, pp. 1027–1053, 2nd. Quart. 2017, doi: 10.1109/COMST.2016.2633387.
- [2] D. Trung, Z. Xiangyun, and H. V. Poor, *Trusted Communications With Physical Layer Security for 5G and Beyond*. London, U.K.: Institution of Engineering and Technology, 2018.
- [3] Z. Wei et al., "Energy- and cost-efficient physical layer security in the era of IoT: The role of interference," *IEEE Commun. Mag.*, vol. 58, no. 4, pp. 81–87, Apr. 2020, doi: 10.1109/MCOM.001.1900716.
- [4] S. Seneviratne et al., "A survey of wearable devices and challenges," *IEEE Commun. Surveys Tuts.*, vol. 19, no. 4, pp. 2573–2620, 4th. Quart. 2017, doi: 10.1109/COMST.2017.2731979.
- [5] J. W. Kim et al., "Collecting Health lifelog data from smartwatch users in a privacy-preserving manner," *IEEE Trans. Consum. Electron.*, vol. 65, no. 3, pp. 369–378, Aug. 2019, doi: 10.1109/TCE.2019.2924466.
- [6] Y. Qadri et al., "The future of healthcare Internet of Things: A survey of emerging technologies," *IEEE Commun. Surveys Tuts.*, vol. 22, no. 2, pp. 1121–1167, 2nd. Quart. 2020, doi: 10.1109/COMST.2020.2973314.
- [7] G. A. Conway and W. G. Scanlon, "Antennas for over-body-surface communication at 2.45 GHz," *IEEE Trans. Antennas. Propag.*, vol. 57, no. 4, pp. 844–855, Apr. 2009, doi: 10.1109/TAP.2009.2014525.
- [8] F. Merli et al., "Design, realization and measurements of a miniature antenna for implantable wireless communication systems," *IEEE Trans. Antennas. Propag.*, vol. 59, no. 10, pp. 3544–3555, Oct. 2011, doi: 10.1109/TAP.2011.2163763.
- [9] D. Gasperini et al., "Matching layer design for far-field and near-field penetration into a multi-layered lossy media [Bioelectromagnetics]," *IEEE Antennas Propag. Mag.*, vol. 64, no. 5, pp. 86–96, Oct. 2022, doi: 10.1109/MAP.2022.3195466.
- [10] M. P. Daly and J. T. Bernhard, "Beamsteering in pattern reconfigurable arrays using directional modulation," *IEEE Trans. Antennas. Propag.*, vol. 58, no. 7, pp. 2259–2265, Jul. 2010, doi: 10.1109/TAP.2010.2046854.
- [11] Y. Ding and V. F. Fusco, "A vector approach for the analysis and synthesis of directional modulation transmitters," *IEEE Trans. Antennas. Propag.*, vol. 62, no. 1, pp. 361–370, Jan. 2014, doi: 10.1109/TAP.2013.2287001.
- [12] A. Babakhani, D. B. Rutledge, and A. Hajimiri, "Transmitter architectures based on near-field direct antenna modulation," *IEEE J. Solid-State Circuits*, vol. 43, no. 12, pp. 2674–2692, Dec. 2008, doi: 10.1109/JSSC.2008.2004864.
- [13] T. Hong, M.-Z. Song, and Y. Liu, "Dual-beam directional modulation technique for physical-layer secure communication," *IEEE Antennas Wireless Propag. Lett.*, vol. 10, pp. 1417–1420, Dec. 2011, doi: 10.1109/LAWP.2011.2178384.
- [14] Y. Ding and V. F. Fusco, "A synthesis-free directional modulation transmitter using retrodirective array," *IEEE J. Sel. Topics Signal Process.*, vol. 11, no. 2, pp. 428–441, Mar. 2017, doi: 10.1109/JSTSP.2016.2605066.
- [15] M. P. Daly and J. T. Bernhard, "Directional modulation technique for phased arrays," *IEEE Trans. Antennas. Propag.*, vol. 57, no. 9, pp. 2633–2640, Sep. 2009, doi: 10.1109/TAP.2009.2027047.
- [16] Q. Zhu et al., "Directional modulation based on 4-D antenna arrays," *IEEE Trans. Antennas. Propag.*, vol. 62, no. 2, pp. 621–628, Feb. 2014, doi: 10.1109/TAP.2013.2290122.
- [17] N. Valliappan, A. Lozano, and R. W. Heath, "Antenna subset modulation for secure millimeter-wave wireless communication," *IEEE Trans. Commun.*, vol. 61, no. 8, pp. 3231–3245, Aug. 2013, doi: 10.1109/TCOMM.2013.061013.120459.
- [18] N. N. Alotaibi and K. A. Hamdi, "Switched phased-array transmission architecture for secure millimeter-wave wireless communication," *IEEE Trans. Commun.*, vol. 64, no. 3, pp. 1303–1312, Mar. 2016, doi: 10.1109/TCOMM.2016.2519403.
- [19] A. Kalantari et al., "Directional modulation via symbol-level precoding: A way to enhance security," *IEEE J. Sel. Topics Signal Process.*, vol. 10, no. 8, pp. 1478–1493, Dec. 2016, doi: 10.1109/JSTSP.2016.2600521.
- [20] Q. Cheng et al., "Time-invariant angle-range dependent directional modulation based on time-modulated frequency diverse arrays," *IEEE Access*, vol. 5, pp. 26,279–26,290, Nov. 2017, doi: 10.1109/ACCESS.2017.2772246.
- [21] M. Hafez et al., "Secure spatial multiple access using directional modulation," *IEEE Trans. Wireless Commun.*, vol. 17, no. 1, pp. 563–573, Jan. 2018, doi: 10.1109/TWC.2017.2768419.
- [22] T. Xie, J. Zhu, and Y. Li, "Artificial-noise-aided zero-forcing synthesis approach for secure multi-beam directional modulation," *IEEE Commun. Lett.*, vol. 22, no. 2, pp. 276–279, Feb. 2018, doi: 10.1109/LCOMM.2017.2772228.
- [23] F. Shu et al., "Robust secure transmission of using main-lobe-integration-based leakage beamforming in directional modulation MU-MIMO systems," *IEEE Syst. J.*, vol. 12, no. 4, pp. 3775–3785, Dec. 2018, doi: 10.1109/JSYST.2017.2764142.
- [24] F. Shu et al., "Secure and precise wireless transmission for random-subcarrier-selection-based directional modulation transmit antenna array," *IEEE J. Sel. Areas Commun.*, vol. 36, no. 4, pp. 890–904, Apr. 2018, doi: 10.1109/JSAC.2018.2824231.
- [25] W.-Q. Wang and Z. Zheng, "Hybrid MIMO and phased-array directional modulation for physical layer security in mmWave wireless communications," *IEEE J. Sel. Areas Commun.*, vol. 36, no. 7, pp. 1383–1396, Jul. 2018, doi: 10.1109/JSAC.2018.2825138.
- [26] Y. Ding, V. F. Fusco, J. Zhang, and W.-Q. Wang, "Time-modulated OFDM directional modulation transmitters," *IEEE Trans. Veh. Technol.*, vol. 68, no. 8, pp. 8249–8253, Aug. 2019, doi: 10.1109/TVT.2019.2924543.
- [27] A. Narbudowicz, M. J. Ammann, and D. Heberling, "Directional modulation for compact devices," *IEEE Antennas Wireless Propag. Lett.*, vol. 16, pp. 2094–2097, Apr. 2017, doi: 10.1109/LAWP.2017.2697720.
- [28] J. Parron, E. A. Cabrera-Hernandez, A. Tennant, and P. de Paco, "Multiport compact stacked patch antenna with 360° beam steering for generating dynamic directional modulation," *IEEE Trans. Antennas. Propag.*, vol. 69, no. 2, pp. 1162–1167, Feb. 2021, doi: 10.1109/TAP.2020.3008065.
- [29] A. Abu Arisheh et al., "A dynamic pattern dipole antenna for secure wireless communications," in *Proc. IEEE Inter. Symp. Antennas Propag. USNC-URSI*, 2022, pp. 1470–1471, doi: 10.1109/AP-S/USNC-URSI47032.2022.9887173.
- [30] A. Zandamela, N. Marchetti, and A. Narbudowicz, "Directional modulation from a wrist-wearable compact antenna," in *Proc. 16th Eur. Conf. Antennas Propag. (EuCAP)*, 2022, pp. 1–5, doi: 10.23919/EuCAP53622.2022.9769624.
- [31] A. Narbudowicz, A. Zandamela, N. Marchetti, and M. J. Ammann, "Energy-efficient dynamic directional modulation with electrically small antennas," *IEEE Antennas Wireless Propag. Lett.*, vol. 21, no. 4, pp. 681–684, Apr. 2022, doi: 10.1109/LAWP.2022.3141212.
- [32] H. Hamouda et al., "Small antenna embedded in a wrist-watch for application in telemedicine," in *Proc. Eur. Conf. Antennas Propag. (EuCAP)*, 2014, pp. 876–879, doi: 10.1109/EuCAP.2014.6901902.
- [33] S.-W. Su and Y.-T. Hsieh, "Integrated metal-frame antenna for smartwatch wearable device," *IEEE Trans. Antennas. Propag.*, vol. 63, no. 7, pp. 3301–3305, Jul. 2015, doi: 10.1109/TAP.2015.2428736.
- [34] Y.-S. Chen and T.-Y. Ku, "A low-profile wearable antenna using a miniature high impedance surface for smartwatch applications," *IEEE Antennas Wireless Propag. Lett.*, vol. 15, pp. 1144–1147, 2016, doi: 10.1109/LAWP.2015.2496366.
- [35] D. Wu and S. W. Cheung, "A cavity-backed annular slot antenna with high efficiency for smartwatches with metallic housing," *IEEE Trans. Antennas. Propag.*, vol. 65, no. 7, pp. 3756–3761, Jul. 2017, doi: 10.1109/TAP.2017.2705223.
- [36] M. Jeon et al., "GPS, Bluetooth and Wi-Fi tri-band antenna on metal frame of smartwatch," in *Proc. IEEE Inter. Symp. Antennas Propag. (APSURSI)*, 2016, pp. 2177–2178, doi: 10.1109/APS.2016.7696795.
- [37] Y. Jia et al., "Miniaturized wearable watch antenna for wristband applications," in *Proc. IEEE*

(continued on page 90)

duties, he served as associate editor of several IEEE journals, such as *IEEE Transactions on Antennas and Propagation*, *IEEE Open Journal of Antennas and Propagation*, *IEEE Transactions on Instrumentation and Measurement*, and *IEEE Antennas and Propagation Magazine*. He was chair of the 2023 IEEE International Conference on Antenna Measurements and Applications and was honorary cochair of the IEEE International Conference on Imaging Systems and Techniques since its establishment in 2004.

In addition to his great scientific accomplishments, Prof. Pastorino was primarily a wonderful person, beloved among all his colleagues and relatives. He was always very sensitive to others' needs, providing help and words of


wisdom to anyone who needed it. He always had a kind word for everyone, in all situations, with a smile to embellish everything. From a didactic perspective, he was a teacher much loved by all of his students. Many of them have found a true passion for science through his enthusiasm in teaching and researching. Prof. Pastorino was always eager to share his knowledge with others—but also his doubts and points of criticism—and to learn from others as well. His kind, humble, and sympathetic character, together with his tenacity, made him an extraordinary example among colleagues and friends. He was always ready to express his gratitude to others, and now we cannot find suitable words to thank him. His death is a tremendous loss to

his family, his friends, and the entire scientific community.

AUTHOR INFORMATION

Andrea Randazzo (andrea.randazzo@unige.it) is with the Department of Electrical, Electronic, Telecommunications Engineering, and Naval Architecture, University of Genoa, I-16145 Genoa, Italy. He is a Senior Member of IEEE.

Andrea Massa (andrea.massa@unitn.it) is with the ELEDIA Research Center, University of Trento, I-38123 Trento, Italy. He is a Fellow of IEEE.

Alessandro Fedeli (Alessandro.fedeli@unige.it) is with the Department of Electrical, Electronic, Telecommunications Engineering, and Naval Architecture, University of Genoa, I-16145 Genoa, Italy. He is a Member of IEEE. 

BIOELECTROMAGNETICS

(continued from page 69)

MTT-S Int. Microw. Biomed. Conf. (IMBioC), 2019, vol. 1, pp. 1–3, doi: 10.1109/IMBIO-OC.2019.8777816.

[38] M.-A. Chung, “Embedded 3D multi-band antenna with ETS process technology covering LTE/WCDMA/ISM band operations in a smart wrist wearable wireless mobile communication device design,” *IET Microw. Antennas Propag.*, vol. 14, no. 1, pp. 93–100, 2020, doi: 10.1049/iet-map.2018.5486.

[39] S. Kumar et al., “A bandwidth-enhanced sub-GHz wristwatch antenna using an optimized feed structure,” *IEEE Antennas Wireless Propag. Lett.*, vol. 20, no. 8, pp. 1389–1393, Aug. 2021, doi: 10.1109/LAWP.2021.3081453.

[40] B. Xiao et al., “Design of small multiband full-screen smartwatch antenna for IoT applications,” *IEEE Internet Things J.*, vol. 8, no. 24, pp. 17,724–17,733, Dec. 2021, doi: 10.1109/JIOT.2021.3082535.

[41] S. Woo et al., “Design of a compact UWB diversity antenna for WBAN wrist-watch applications,” in *Proc. Int. Symp. Antennas Propag.*, 2013, vol. 2, pp. 1304–1306.

[42] W.-S. Chen et al., “MIMO antenna with Wi-Fi and Blue-Tooth for smart watch applications,” in *Proc. IEEE MTT-S Int. Microw. (IMWS-BIO)*, 2015, pp. 212–213, doi: 10.1109/IMWS-BIO.2015.7303852.

[43] J. Chen et al., “A multiple antenna system design for wearable device using theory of char-

acteristic mode,” in *Proc. Eur. Conf. Antennas Propag. (EuCAP)*, 2018, pp. 1–5, doi: 10.1049/cp.2018.0430.

[44] D. Wen et al., “Design of a MIMO antenna with high isolation for smartwatch applications using the theory of characteristic modes,” *IEEE Trans. Antennas Propag.*, vol. 67, no. 3, pp. 1437–1447, Mar. 2019, doi: 10.1109/TAP.2018.2884849.

[45] B. Wang and S. Yan, “Design of smartwatch integrated antenna with polarization diversity,” *IEEE Access*, vol. 8, pp. 123,440–123,448, Jun. 2020, doi: 10.1109/ACCESS.2020.3006076.

[46] C.-T. Liao, Z.-K. Yang, and H.-M. Chen, “Multiple integrated antennas for wearable fifth-generation communication and Internet of Things applications,” *IEEE Access*, vol. 9, pp. 120,328–120,346, Aug. 2021, doi: 10.1109/ACCESS.2021.3107730.

[47] L. Chen et al., “An efficient directional modulation transmitter with novel crest factor reduction technique,” *IEEE Microw. Wireless Compon. Lett.*, vol. 29, no. 8, pp. 554–556, Aug. 2019, doi: 10.1109/LMWC.2019.2923361.

[48] J. M. Purushothama et al., “Synthesis of energy efficiency-enhanced directional modulation transmitters,” in *Proc. IEEE Trans. Green Commun. Netw.*, vol. 7, no. 2, pp. 635–648, Jun. 2023, doi: 10.1109/TGCN.2022.3208023.

[49] G. Huang, Y. Ding, and S. Ouyang, “Multicarrier directional modulation symbol synthesis using

time-modulated phased arrays,” *IEEE Antennas Wireless Propag. Lett.*, vol. 20, no. 4, pp. 567–571, Apr. 2021, doi: 10.1109/LAWP.2021.3056962.

[50] J. Hou et al., “Energy efficient time-modulated OFDM directional modulation transmitters,” *Microw. Opt. Technol. Lett.*, vol. 65, no. 1, pp. 5–13, 2023, doi: 10.1002/mop.33438.

[51] R. J. Maughan, J. S. Watson, and J. Weir, “The relative proportions of fat, muscle and bone in the normal human forearm as determined by computed tomography,” *Clin. Sci.*, vol. 66, no. 6, pp. 683–689, Jun. 1984, doi: 10.1042/cs0660683.

[52] C. Gabriel, “Compilation of the dielectric properties of body tissues at RF and microwave frequencies,” Defense Technical Information Center, Fort Belvoir, VA, USA, Brooks Air Force Tech. Rep., AL/OE-TR-1996-0037, 1996.

[53] A. Zandamela, N. Marchetti, M. J. Ammann, and A. Narbudowicz, “Spherical modes driven directional modulation with a compact MIMO antenna,” *IEEE Antennas Wireless Propag. Lett.*, vol. 22, no. 3, pp. 477–481, Mar. 2023, doi: 10.1109/LAWP.2022.3215707.

[54] J. E. Hansen, Ed., *Spherical Near-Field Antenna Measurements* (ser. Electromagnetic Waves). London, U.K.: Institution of Engineering and Technology, 1988. [Online]. Available: <https://digital-library.theiet.org/content/books/ew/pbew026e>

